Journal of Materials Chemistry B

Accepted Manuscript

ROYAL SOCIETY OF CHEMISTRY

www.rsc.org/materialsB

Journal of Materials Chemistry B RSCPublishing

ARTICLE

Conductive Composite Fibres from Reduced Graphene Oxide and Polypyrrole Nanoparticles

K.S.U. Schirmer[a], D. Esrafilzadeh[a,b], B.C. Thompson[a, c], A.F. Quigley[a, d], R.M.I. Kapsa[a,d] and G.G. Wallace[a*]

Cite this: DOI: 10.1039/x0xx00000x

Received 00th January 2012,
Accepted 00th January 2012

DOI: 10.1039/x0xx00000x

www.rsc.org/

Continuous composite fibres composed of polypyrrole (PPy) nanoparticles and reduced graphene oxide (rGO) at different mass ratios were fabricated using a single step wet-spinning approach. The electrical conductivity of the composite fibres increased significantly with the addition of rGO. The mechanical properties of the composite fibres also improved by the addition of rGO sheets compared to fibres containing only polypyrrole. The ultimate tensile strength of the fibres increased with the proportion of rGO mass present. The elongation at break was greatest for the composite fibre containing equal mass ratios of PPy nanoparticles and rGO sheets. L929 fibroblasts seeded onto fibres showed no reduction in cell viability. To further assess toxicity, cells were exposed to media that had been used to extract any aqueous-soluble leachates from developed fibre. Overall, these composite fibres show promising mechanical and electrical properties while not significantly impeding cell growth, opening up a wide range of potential applications including nerve and muscle regeneration studies.

Introduction

Over the last three decades, significant progress has been made in achieving regeneration of damaged peripheral nerve tissue[1-3]. Much of the progress can be attributed to the improvement in biomaterials and scaffolds as well as the increased understanding of factors that support the natural ability of the nerve to regenerate[4-9]. Mechanical properties of materials for scaffold development need to be selected carefully to suit the application as well as enable fabrication into structures of the required size and shape. The materials should mimic the natural tissue, guide and stimulate cells using electrical[10-12], chemical[13-17] and physical[7, 18-20] cues [21, 22]. Fibres and fibrous structures, ranging from nanoscale to microscale, have been increasingly used for nerve regenerative applications as they best mimic the natural structure of nerves, providing guidance to the regenerating axons, resulting in faster reconnection of the regenerating tissue[23-26]. Biomaterials with electrical conductivity allow electrical stimulation of cells and tissues, which is known to have positive effects on neural regeneration, resulting in longer neurite outgrowth and alignment[13, 26, 27].

Polypyrrole (PPy) has been used extensively for regenerative nerve applications[28, 29]. The conducting nature, simplicity of synthesis and biocompatibility of PPy has led to its use in triggering controlled drug delivery as well as applying electrical stimulation to cells and tissues. [26-28, 30-35]. PPy can be synthesized *via* chemical or electrochemical polymerization, resulting in generally insoluble powders or thin films[36]. Chemical polymerization in the presence of a stabiliser produces colloids in the size range 10 – 100 nm[37]. These PPy particles can be dispersed in a number of solvents and mixed with other materials and matrices to form composites. In our previous studies a colloidal synthesis approach was utilized to form conducting PPy particles, which were then fabricated into PPy fibres using a simple wet extrusion technique[38]. The resulting fibres exhibited poor mechanical properties, no measurable conductivity and low electroactivity due to a lack of interactions between nanoparticles[38]. To increase the mechanical and electrochemical properties of the fibres, we have undertaken fabrication of composite materials containing both PPy nanoparticles and graphene. Graphene is a two dimensional, atomic carbon lattice with extraordinary strength and the ability to conduct electricity. It has been commonly used in composites with conducting polymers to enhance their

a ARC Centre for Electromaterials Science and Intelligent Polymer Research Institute, AIIM Facility, Innovation Campus, University of Wollongong, Australia.
b Illawarra Health and Medical Research Institute, University of Wollongong, Australia
c School of Mechanical and Aerospace Engineering, Nanyang Technological University, Singapore.
d Department of Clinical Neurosciences, St Vincent's Hospital, Melbourne and Department of Medicine, The University of Melbourne, Australia.

properties[39-41]. Composites containing both graphene and PPy have found application as capacitors[42-47], sensors[48-50] and electrodes[51, 52]

There are different types of graphite (multi-layer stacks) and graphene (single layer), which exhibit a range of mechanical and electrical properties[53, 54]. Graphite oxide is highly oxidized and has oxygenated functionalities within its structure, which not only increase the distance between the layers but also make it hydrophilic and more dispersible in water than non-functionalized graphite[55]. This property enables graphite oxide to be exfoliated in water ultimately producing single or few layer graphene oxide (GO)[55-57]. The dispersibility of GO in both aqueous and organic solvents is a desirable property for fabrication of composites, as mixing with other materials can easily be achieved[58]. The oxidation of graphene results in a disruption of its sp^2 bonding networks, and accordingly GO is an electrical insulator. To achieve electrical conductivity, the sp^2 bonds need to be restored, which requires reduction of the GO[53, 55-57, 59, 60]. GO can be reduced using thermal, chemical and electro-chemical reduction, leading to the removal of oxygen-containing functional groups and restoring most of the sp^2 bonds[56, 60]. Reduced GO (rGO) can conduct electricity[61], but is more difficult to disperse and has a tendency to re-aggregate as a result of the removal of oxygen groups[53, 62].

Two approaches to form composite materials from GO and PPy have been primarily used in previous studies. In one of these approaches PPy is synthesized, forming films, nanowires or particles, prior to mixing with GO[47, 48, 63, 64]. The other approach requires mixing of pyrrole monomer and GO prior to the synthesis of PPy, which is then performed *in situ*[65-71].

Recent work by Ding *et al.*[67] describes the fabrication of graphene/polypyrrole composite fibres, using an *in situ* spinning approach in which pyrrole and GO are mixed and extruded into baths containing ferric chloride and hydriodic acid. This method results in polymerization to polypyrrole allowing the formation of a continuous fibre and reduction of GO to rGO[67].

In the present work, we demonstrate a simple, single step wet-spinning approach based on mixtures of liquid crystal graphene oxide (LCGO) and PPy nanoparticles to produce continuous, conducting fibres. Furthermore we investigate the electrical, electrochemical and mechanical properties of the fibres and the cytotoxicity of fibres and their leachates.

Experimental

Polypyrrole Nanoparticle and Fibre Synthesis

To synthesize PPy nanoparticle dispersions, 0.5 wt% polyvinyl alcohol (PVA, Sigma, molecular weight 31–50kDa) was stirred in deionised water at 80°C until fully dissolved. The solution was cooled to 4°C before 0.05 M of iron (III) para-toluenesulfonate (FepTS, Sigma) was added to the PVA solution and stirred until dissolved. 0.1 M of pyrrole monomer (Merck, distilled) was slowly added to the cooled PVA solution under continuous stirring and left to polymerize and oxidize for 8 to 12 h before the solution was dialysed against deionized water using dialysis tubing (Sigma, 12 kDa molecular weight cut off). Dialysis was carried out for 48 h with three water changes. The particles were purified after synthesis using cellulose membrane centrifugation tubes (Merck) with a molecular weight cut off of 100 kDa.

Fabrication of PPy fibres was achieved using previously described methods[38]. Briefly, spinning solutions were prepared by gradual addition of 12 wt% freeze-dried PPy nanoparticles to dichloroacetic acid (DCAA). A 3D-Bioplotter (Envisiontec, Manufacturer Series) with a 21-gauge tip was used to extrude the fibres into a deionised water bath (18.2 MΩ cm^{-1}) cooled to 10°C (Figure 1A). After extrusion, the fibres were left in the water bath until solidified, before washing in a series of ethanol/water solutions, (100% ethanol, 75% ethanol in water, 50% ethanol in water, 25% ethanol in water, 10% ethanol in water and water only). Fibres remained in each ethanol bath for 4 h and the final water bath overnight. After the final washing step, fibres were dried under vacuum at 60°C.

rGO – Polypyrrole Composite Fibre Synthesis

Dry expandable graphite flakes (3772, Asbury Graphite Mills USA) were thermally treated (at 1050°C for 15 s) before being used as a precursor for GO synthesis following a previously described method[58, 72]. Briefly, expanded graphite and sulphuric acid were mixed and stirred, before $KMnO_4$ was added to the mixture slowly. The mixture was transferred into an ice bath, before deionised water and H_2O_2 were slowly added to the mixture, resulting in a colour change of the suspension to light brown. After stirring for another 30 min, the GO particles were washed and centrifuged in a HCl solution, before further centrifugation and washing with deionised water, until the solution pH reached 5. The resulting GO sheets were dispersed in deionized water by gentle shaking to form a liquid crystalline graphene oxide dispersion (LCGO)[73, 74].

LCGO (8.7 mg ml^{-1} in water) was stirred overnight with PPy nanoparticle dispersions (100 mg ml^{-1} in water) to achieve final mass ratios of GO:PPy of 80:20, 50:50 and 30:70. Wet-spinning was carried out using a rotational wet-spinning apparatus in a mixture of ethanol and water (70%:30%), 5 wt% calcium chloride and 5 wt% hypophosphorous acid with an extrusion rate of 25 ml h^{-1} using a metal spinneret (20 gauge, Figure 1B). Fibres were kept in the coagulation bath at 90°C for 4 h, before collecting and washing with ethanol as described for PPy fibres.

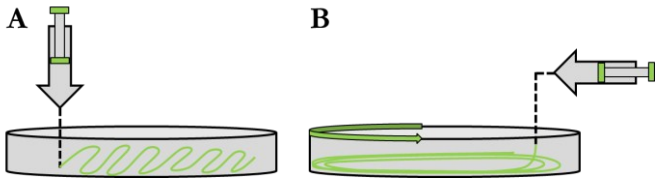

Figure 1: Schematic of extrusion method of polypyrrole fibres (A) and rotation wet spinning of fibres containing graphene (B).

Composite Crystallinity

Formation of liquid crystals of GO and its composites with PPy were evaluated using cross polarized optical microscopy (Leica, CTR6000 and corresponding software LAS version 4.4.0.). A drop of each mixture was placed on a microscope glass slide and observed under the polarized optical microscope, operated in transmission mode. Images were taken at 200x magnification with the analyzer and polarizer perpendicular to each other.

Fibre Characterization

Tensile Testing. Tensile testing was performed using a Shimadzu EZ-S. A minimum of 10 samples were tested for each fibre type, with a sample distance of 1 cm and a sample rate of 1 mm min^{-1} using a 10 N load cell. The elastic modulus was calculated from the linear elastic region in the stress – strain curve. The curves presented are representative for the test results of each fibre type.

Scanning Electron Microscopy (SEM) After tensile testing, fracture surfaces of PPy fibres were sputter-coated with 15 nm of gold before images were taken with a JEOL JSM-7500-FA cold field emission gun scanning electron microscope (FEGSEM, Jeol, Germany). Fracture surfaces of fibres containing rGO were imaged without further surface preparation.

Electroactivity and Conductivity. Cyclic Voltammetry (CV) was used to determine the electroactivity and redox potential of the fibres. The fibres were used as the working electrode in a standard three-electrode set-up, using platinum mesh as the counter electrode and an Ag|AgCl (saturated KCl) reference electrode. All CVs were performed on 1 cm length of fibre in water and 0.1 M phosphate buffered saline (PBS). The potential was scanned between -0.8 and 0.8 V vs. Ag|AgCl at scan rates between 10 and 100 mV sec^{-1}. The weight of each fibre was determined and all CVs were normalized for the mass of the fibre. Data below shows CVs recorded at 25 mV sec^{-1} in PBS. Fibre conductivity was measured for at least 15 samples from different batches per group using a four point probe to which the fibres were attached using silver paint. To investigate the stability of the conductivity, a constant voltage of 25 mV was applied to a 1 cm fibre length for 1 minute before a drop (100 µl) of PBS was added to the middle of the fibre. Changes in current were recorded until the current remained constant.

Fibre Toxicity Testing

To investigate the cytocompatibility of the fibres with L929 fibroblasts, cells were seeded onto the fibres as well as cultured in different concentrations of fibre leachates. L929 fibroblasts were routinely cultured following standard protocols from the American Type Culture Collection (ATCC)[75].

Washed and dried fibres were cut into 5 mm length and sterilized (autoclaved) before washing in Dulbecco's Modified Eagle's Medium (DMEM, Gibco, Life Technologies) twice for 24 hours at 37°C to wet the fibres in the cell culture media. Three 5 mm lengths of fibres were placed into separate wells of a 96-well plate and left to settle in DMEM for 4 hours before L929 fibroblasts were seeded on the fibres at a density of 12000 cells cm^{-2}. L929 cells were left to proliferate for 72 hours without media changes before staining to visualize viability using calcein AM (Life Technologies) and propidium iodide (PI, Life Technologies) and imaged using Axio Vert microscope and corresponding software.

To investigate the possibility that the fibres could release toxic products (leachates) that affect cell viability, L929s were exposed to different concentrations of leachate collected from the different fibre types. Washed and dried fibres were weighed and sterilized (autoclaved) before 7 day incubation in DMEM at 37°C and 5% CO_2 at a concentration of 100 mg mL^{-1}. After 7 days, DMEM was removed from the vials and the pH of the conditioned DMEM was measured. If pH was below 7, it was adjusted using 0.1 M sodium hydroxide. Conditioned DMEM was then filter sterilized using 0.2 µm syringe filters, before addition of 10% Foetal Bovine Serum (FBS, Invitrogen). Cells were seeded at 5000 cells cm^{-2} and left to adhere overnight, before media was removed and replaced with different concentrations of conditioned media (undiluted at 100 mg ml^{-1} fibre, and conditioned media diluted with cell media (DMEM, 10% FBS to 80, 65, 50, 10 and 1 mg ml^{-1}). A positive media-only control and a negative control of media adjusted to pH 2, were used, and all conditions were performed in triplicate. After 24, 48 and 72 h of culturing cells in conditioned media, the media was removed and cells stained to visualize viability as described above.

For analysis of cell viability, live and dead cell numbers were estimated using the cell counter macro available in ImageJ. One-way ANOVA was performed to determine significant differences between treatment groups (alpha level 0.05) using Origin Pro 9.1.0.

Results and Discussion

We have exploited the inherent self-assembly properties of LCGO to induce liquid crystallinity in PPy nanodispersions in

order to improve the properties of PPy nanoparticle fibres. LCGO was introduced into PPy nanodispersions at different weight ratios (LCGO:PPy: 80:20, 50:50 and 30:70). Cross-polarized optical microscopy images (POM) were obtained and show anisotropic, birefringence properties typical for LCGO (Supplementary Figure S1), while the PPy dispersion displays isotropic behaviour. We suggest that the small size of the PPy nanoparticles (50-70 nm) allows them to fit in between the LC mesogens and minimise any disruption of the LC phase. This allows the formation of a LC phase even after the addition of more than double the amount of PPy nanoparticles by weight to the LCGO dispersion. Fibres were successfully produced from rGO, PPy, 80:20 and 50:50 (rGO:PPy, Figure 2), following preliminary wet spinning experiments using a Ca^{2+} containing coagulation bath to spin fibres from LCGO[73]. Fibres were also formed from the spinning solution with a ratio of 30:70, however even after extended coagulation time, the fibres were not strong enough to be handled when removed from the coagulation bath. The coagulation of the fibres is based on ionic crosslinking between the negatively charged rGO sheets and

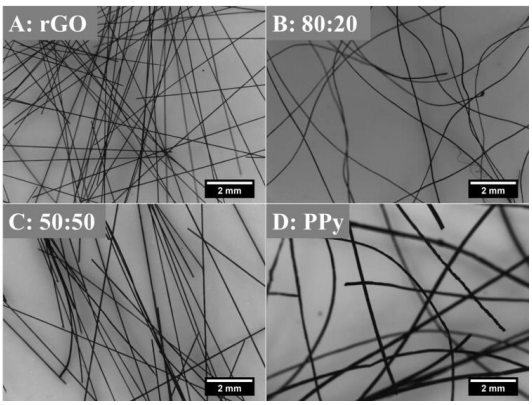

Figure 2: Fibres made from reduced graphene oxide (rGO, A), polypyrrole nanoparticles (PPy, D) and their composites (rGO:PPy) 80:20 (B) and 50:50 (C).

Ca^{2+} ions. The greater physical distance between the rGO sheets induced by an increased PPy content would decrease the degree of cross linking. Fibres produced from rGO, 80:20, 50:50 and PPy are uniform in diameter and were easily produced in continuous lengths of at least 50 cm. Fibres containing graphene were extruded using a 20 gauge needle (600 µm internal diameter). Resulting diameters ranged from 41 ± 6 µm (rGO) to 55 ± 5 µm (80:20) and 61 ± 4 µm (50:50). With more PPy particles present in the fibres containing graphene, less shrinking of the fibres is observed, supporting the hypothesis that the particles increase the spacing between the graphene sheets resulting in less crosslinking points. Fibres fabricated from PPy were 146 ± 24 µm in diameter (extruded from a 21 gauge needle, 510 µm internal diameter).

Electrical and electrochemical properties. The conductivity of the fibres, measured using the four-point-probe method, increased with increasing rGO content. PPy fibres show no measurable conductivity due to the insulating PVA shell around the particles as previously described[38]. However, the lack of electrical conductivity was addressed by the addition of rGO sheets into the fibres. The conductivity of the composite fibres increased significantly after the addition of 50 wt% and 80 wt% rGO (18 ± 4 S cm^{-1} to 20 ± 3 S cm^{-1}), respectively. The conductivity of these fibres is possibly generated through the interconnected pathways created by the rGO sheets. An increase in PPy particle content, likely increases the distance between the rGO sheets, which results in a reduction of the conductivity compared to fibres containing only rGO (30 ± 6 S cm^{-1}). The conductivity values reported here are an order of magnitude higher than measured for previously reported rGO and PPy fibres (~ 1.4 S cm^{-1})[67]. This can be explained by the high alignment of rGO sheets within the fibres, resulting from the liquid crystalline phase of the spinning solution. The stability of the conductivity upon hydration was investigated by exposing dried 80:20 fibres to PBS while applying 25 mV and recording the resulting current. After a droplet of PBS came into contact with the dried fibre the current increased briefly before dropping and finally stabilizing at around 40% of the original value (Supplementary Figure S2) indicating stable, albeit reduced, conductivity of the fibres within a media mimicking physiological conditions .

Cyclic Voltammetry (CV) was performed to determine the electrochemical behaviour of the fibres comprised of rGO, PPy and their composites (Figure 3). The electrochemical studies using a three-electrode configuration setup demonstrate a highly resistive response for fibre made entirely from PPy nanoparticles (Figure 3 insert), compared to fibres containing rGO. This behaviour is postulated to be a result of the insulating PVA around the nanoparticles[38], which makes them electrochemically inaccessible. When mixed with rGO, electrical conductivity is introduced into the fibres, resulting in a pronounced capacitive electrochemical response, however typical PPy peaks cannot be identified in the CVs.

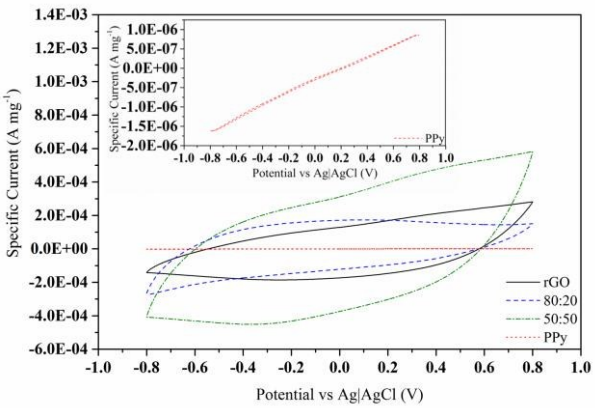

Figure 3: Cyclic Voltammetry (CV) of reduced graphene oxide (rGO, solid black) fibres, polypyrrole (PPy, dotted red, enlarged in insert) nanoparticle fibres and their composite fibres (rGO:PPy) 80:20 (dashed blue) and 50:50 (dash-dotted green). CVs were recorded in a standard 3 electrode setup, using the fibre as the working electrode, platinum mesh as the counter and Ag|AgCl as the reference electrode. CVs shown here are representative and were recorded at 25 mV sec^{-1} against Ag|AgCl in phosphate buffered saline (PBS).

A decrease in rGO content results in less capacitive fibres, with the greatest capacitance observed in the 50:50 composite fibres (as demonstrated by the increased charging current represented by the distance between the forwards and backwards scan), while the capacitance of rGO and 80:20 composite fibres is similar. All fibres exhibit a voltage dependency of the current, indicating that Faradaic processes are occurring. Since the overall porosity and morphology of the fibres is very similar, geometric and surface area effects on the electrochemical response are believed to be minimal. A similar electrochemical behaviour of rGO/PPy composite fibres has been reported by Ding *et al.*[67].

Mechanical Properties. To evaluate the mechanical properties of the composite fibres, in comparison to the fibres containing only PPy or rGO, tensile testing was performed on all fibres. Representative Stress - Strain curves (Figure 4) demonstrate that all fibres initially display a linear elastic behaviour. The strength of the fibres increased with an increase in rGO content. Fibres made from PPy were the weakest, with an elastic modulus of 0.5 ± 0.2 GPa, while the 50:50 composite fibres showed the greatest strength and ductility. There was no significant difference in ductility between rGO, 80:20 and PPy fibres (Figure 4). There is no difference in the elastic modulus of the composite fibres 80:20 and 50:50, showing values of 8 ± 4 GPa and 8 ± 3 GPa, respectively. The rGO fibres show the highest elastic modulus (13 ± 4 GPa) and ultimate stress (175 ± 8 MPa), but a lower elongation at break compared to 50:50 with a maximum strain of 6.9% ± 0.3%. It is hypothesized that the higher elongation at break of the 50:50 composite is a result of the composition, which could allow sliding and aligning of graphene sheets with the PPy particles acting as a lubricant.

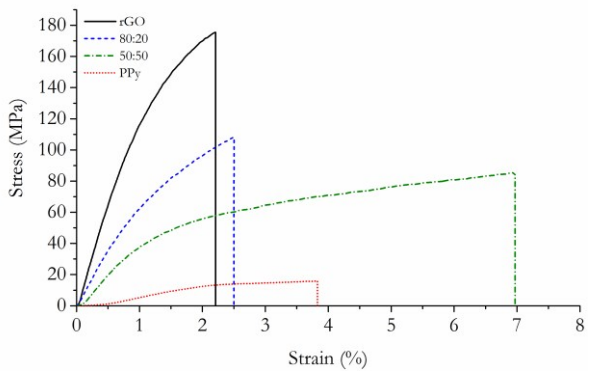

	Elastic Modulus [GPa]	Max Stress [MPa]	Max Strain [%]	Conductivity [S cm^{-1}]
rGO	13 ± 4	175 ± 8	2.2 ± 0.5	30 ± 6
80:20	8 ± 4	110 ± 20	2.5 ± 0.7	20 ± 3
50:50	8 ± 3	90 ± 30	6.9 ± 0.3	18 ± 4
PPy	0.5 ± 0.2	10 ± 7	4 ± 3	-

Figure 4: Material properties of fibres containing reduced graphene oxide (rGO), polypyrrole (PPy) and their composites (rGO:PPy, 80:20 and 50:50). A: Stress - Strain curve. B: Summary of tensile properties of all fibre types and their conductivity.

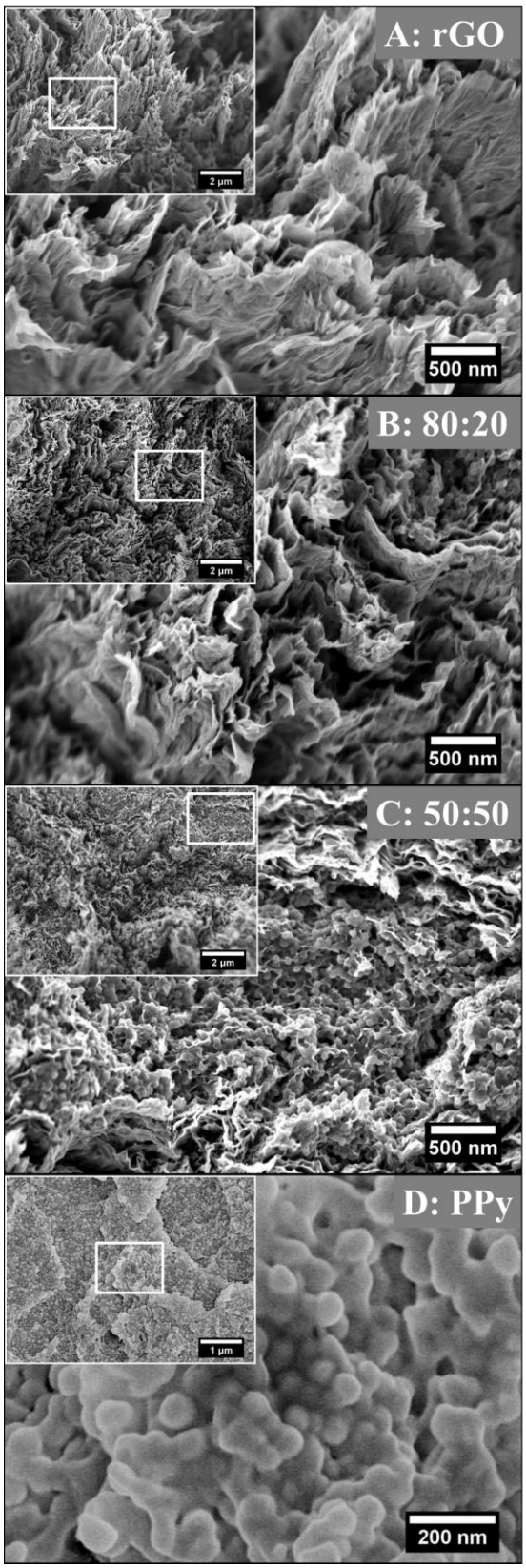

Figure 5: Scanning electron microscopy cross section images fibres synthesized from reduced graphene oxide (A: rGO), polypyrrole nanoparticles (D: PPy) and their composites at rGO:PPy ratios of 80:20 and 50:50. Cross sections were analysed after tensile testing (PPy fibres were sputter coated with gold to facilitate imaging).

The comparably high variation within the PPy fibre group is most likely caused by defects within the fibres which have significant impact on the failure behaviour during tensile testing. As the fibres contain a matrix (PVA) that makes up less than 50% of the overall mass of the fibre, small irregularities like particle agglomerations will introduce significant defects into the fibres. Upon addition of rGO to the PPy fibres, the variation within the sample groups decreases drastically, as the increase in mechanical properties is a result of the interactions between rGO sheets, which are much less affected by defects in the structure.

In comparison to previous work the fibres described here show similar or better mechanical properties compared to the graphene-polypyrrole fibres fabricated by Ding *et al.*[67], indicating that the incorporation of PPy results in reduced mechanical strength, regardless of the morphology of the PPy components.

Scanning Electron Microscopy Imaging. SEM images of the fracture surfaces after fatal tensile testing were obtained. Figure 5 shows lower (insert) and higher magnification images of all fibre cross sections. These images demonstrate that the PPy particles are distributed homogeneously both on the surface of the rGO sheets and also between the sheets. Sheets of graphene and spherical polypyrrole particles can be clearly identified in all fibres containing either or both components. All fibres appear to be solid, with low porosity and homogeneous in their internal structure and distribution.

Fibre Toxicity. To examine the cytocompatibility of the fibres, L929 fibroblast cells were seeded directly onto the fibres, as well as cultured in media containing fibre leachates (Figure 6).

L929 fibroblasts seeded directly on the fibres were allowed to grow for 3 days before cell viability was analysed (Figure 6A). Cell viability was found to range between 98 – 99% on all samples, with no differences found in number of live or dead cells between the samples. Most importantly, none of the samples showed a decrease in viability compared to cell media (cells grown on tissue culture plastic) controls. Cells were found to adhere to all types of fibres as can be seen from representative images shown in Figure 6A.

To investigate the effect of potential leachates at higher fibre concentrations, fibre compositions were incubated in DMEM at 37°C and 5% CO_2 to generate media conditioned with leached products. The conditioned media was then used to culture L929 cells in order to evaluate the potential toxicity of leachates from the fibres. Cells were exposed to varied concentrations of the conditioned media over periods of 1, 2 and 3 days before an estimation of live and dead cells was determined for each treatment group. The graph in Figure 6B shows the number of live and dead cells, exposed to the equivalent of media conditioned with low (1 mg ml^{-1}), medium (50 mg ml^{-1}) and high (100 mg ml^{-1}) concentrations of fibres after 48 hours (see Supplementary Figure S3 for all time points and concentrations). Cells were also exposed to normal unconditioned media (positive control) as well as a media control adjusted to pH 2 (negative control).

After incubation of media with the different fibres, the pH of the conditioned media was found to range between 7 and 7.4 for rGO, 80:20 and 50:50 fibres, which is a slight reduction in pH compared to unconditioned DMEM (pH 7.5). This is likely the result of leaching of some acidic reagent from the spinning bath, however differences were found to be minimal so pH was not adjusted before cell culture. DMEM incubated with PPy fibres showed a pH of 2. To adjust the pH to 7.5, 150 µL of 0.1 M NaOH was added. The low pH in the conditioned media was most likely caused by residual DCAA in the PPy fibre after synthesis and washing.

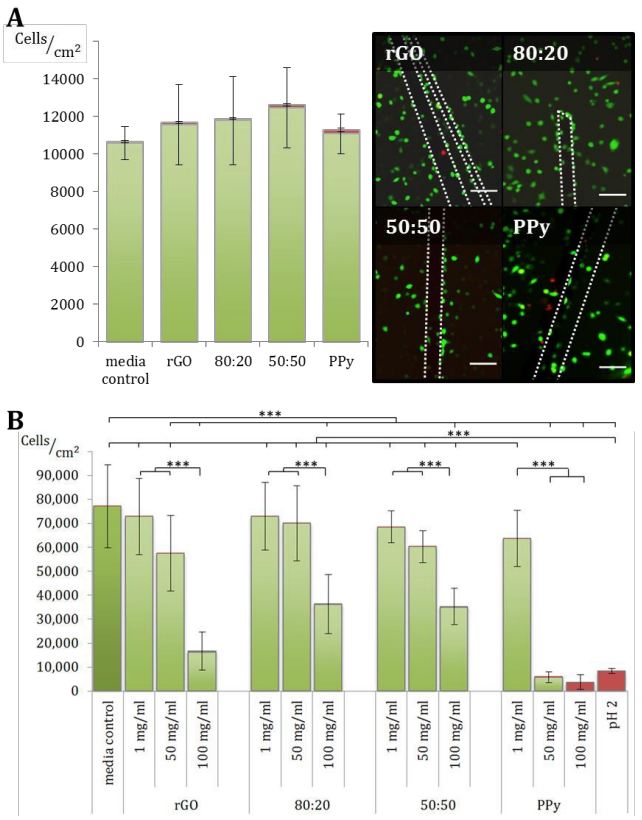

Figure 6: A: Live (green) and dead (red) cell numbers of L929 cells after 3 days of culturing on fibres and representative images of stained cells attached to fibres. White dotted lines mark the fibre outlines. B: Live (green) and dead (red) cell numbers of L929 cells after 2 days of culturing in media conditioned with 1 mg ml^{-1}, 50 mg ml^{-1} and 100 mg ml^{-1} reduced graphene oxide (rGO) fibres, polypyrrole (PPy) fibres and composites (rGO:PPy) 80:20 and 50:50. Error bars indicate the standard deviation. Selected relevant significant differences are indicated (* = p<0.05, ** = p<0.01, *** = p<0.001) Bottom: To top graph corresponding representative images of live (green) and dead (red) stained cells cultured in conditioned media containing the equivalent of 1 mg ml^{-1} (1) and 100 mg ml^{-1} (100) of each fibre type respectively. Scale represents 100 µm.

After 48 hours, no significant decrease in number of live L929 cells was found when exposed to conditioned media containing leachates from 1 mg ml^{-1} of any fibre type, compared to the media-only control. Furthermore, the number of live cells was not reduced significantly when cultured in the conditioned media containing leachates from 50 mg ml^{-1} of composite fibres 80:20 and 50:50.

The number of live cells was significantly reduced when cells were cultured in conditioned media containing leachates from 50 mg ml^{-1} and 100 mg ml^{-1} of rGO or PPy fibre, or leachates from 100 mg ml^{-1} of composite fibres 80:20 or 50:50.

For cells cultured in media conditioned with 1 mg ml^{-1} or 50 mg ml^{-1} of fibres containing rGO (rGO, 80:20 and 50:50), the number of live cells was significantly higher compared to cells cultured in leachates produced from 100 mg ml^{-1} of these fibres. Cells cultured in media containing leachates derived from either 50 mg ml^{-1} or 100 mg ml^{-1} PPy fibres, showed significantly reduced viability compared to cells cultured in media conditioned with 1 mg ml^{-1} of PPy fibres. This strongly suggests that pure PPy fibres show significantly increased toxicity at lower doses (50 mg ml^{-1}) compared to fibres containing rGO.

It is important to note that the ratio of dead cells was very low for all samples and treatment groups (0.3 – 1.2% of live cells), except for cells exposed to leachates derived from PPy, even though the number of live cells was reduced significantly between and across the treatment groups. The consistently low number of dead cells could be caused by cells being washed off during the staining procedure. This effect would also be amplified by a decreased rate of cell proliferation.

Cells cultured in conditioned media containing the leachates from 50 mg ml^{-1} or 100 mg ml^{-1} of PPy showed 8 % and 100% dead cells, respectively. By adjusting the pH of the conditioned media to pH 7.5, the osmolarity of the media was changed, which could be a contributing factor to the high amount of dead cells. The same applies for the negative pH 2 control, which exposed the cells to not only a pH of 2, but also changes in osmolarity.

Overall the media conditioned with composite fibres 80:20 and 50:50 seem to be tolerated best by L929 cells. The fibres showed no sign of degradation after being incubated at 37°C in media for 7 days, the media was clear and no aggregates were visible. The slight decrease in pH can contribute to the changes in cell proliferation and cell number, however it is possible that vital nutrition components, such as essential amino acids or vitamins and inorganic salts adhered to the fibres during incubation and were as a result, reduced or missing in the conditioned media. Furthermore, non-acidic fibre components could have leached out of the fibres and affected cell metabolism. Overall the cells tolerated media incubated with more than 1.5 m of the fibres per ml, which exceeds the lengths usually utilized in *in vivo* applications. Nonetheless, further investigation needs to be carried out to determine the biocompatibility of rGO/PPy composite fibres, particularly the investigation of application-specific cell-type compatibility and effects on cells directly in contact with the fibres *in vivo*.

Conclusions

Composite fibres made from reduced graphene oxide (rGO) and polypyrrole (PPy) nanoparticles have been produced using a simple one step wet-spinning approach. The fibres show superior conductivities and mechanical properties compared to similar composite fibres reported in the literature. While fibres containing both rGO and PPy showed great improvements in mechanical and electrical properties compared to PPy fibres, composite fibres were generally inferior to rGO fibres. The toxicity of fibres and fibre leachates was also investigated. L929 fibroblasts cultured on fibres showed no significant change in cell viability or number, while cell viability and number was affected when cultured in high concentrations of fibre leachates, with the composite fibres showing the least toxicity. The high-level conductivity, mechanical properties as well as cytotolerance make these composite fibres suitable for a wide range of applications including as cell scaffolding components in implantable devices that involve electrical stimulation. Fibres can be used in the form of freestanding 3D structures that can simultaneously act as a scaffold and conductor for electrical stimulation.

Acknowledgements

The authors would like to thank the ARC Australian Laureate Fellowship scheme and the Australian Institute for Innovative Materials (AIIM) for funding, the Australian National Fabrication Facility (ANFF) for providing access to facilities, instruments and staff. The authors would also like to thank Dr Elise Stewart for assistance with cell toxicity analysis and Dr Rouhollah Jalili for synthesis of graphene oxide dispersion. The authors acknowledge the use of the facilities and the assistance of Mitchell Nancarrow at the UOW Electron Microscopy Centre.

Electronic Supplementary Information (ESI) available: Figure S1: Polarized optical microscopy images of spinning solutions. Figure S2: Stability of fibre conductivity. Figure S3: numbers of live and dead cells over 3 time points, incubated with different concentrations of conditioned media. See DOI: 10.1039/b000000x/

References

1. C. McCaig and A. Rajnicek, *Experimental Physiology*, 1991, **76**, 473-494.
2. T. Hadlock, J. Elisseeff, R. Langer, J. Vacanti and M. Cheney, *Arch Otolaryngol Head Neck Surg*, 1998, **124**, 1081-1086.
3. A. Hart, G. Terenghi and M. Wiberg, in *Tissue Engineering*, eds. N. Pallua and C. V. Suscheck, Springer Berlin Heidelberg, 2011, DOI: 10.1007/978-3-642-02824-3_13, ch. 13, pp. 245-262.

4. T. B. Bini, S. Gao, S. Wang and S. Ramakrishna, *J Mater Sci Mater Med*, 2005, **16**, 367-375.
5. A. Subramanian, U. M. Krishnan and S. Sethuraman, *Journal Of Biomedical Science*, 2009, **16**, 108-108.
6. X. Jiang, S. H. Lim, H.-Q. Mao and S. Y. Chew, *Experimental Neurology*, 2010, **223**, 86-101.
7. M. Sun, M. McGowan, P. J. Kingham, G. Terenghi and S. Downes, *J Mater Sci Mater Med*, 2010, DOI: 10.1007/s10856-010-4120-7.
8. W. Daly, L. Yao, D. Zeugolis, A. Windebank and A. Pandit, *Journal of The Royal Society Interface*, 2011, **9**, 202-221.
9. A. F. Quigley, K. J. Bulluss, I. L. B. Kyratzis, K. Gilmore, T. Mysore, K. S. U. Schirmer, E. L. Kennedy, M. O. Shea, Y. B. Truong, S. L. Edwards, G. Peeters, P. Herwig, J. M. Razal, T. E. Campbell, K. N. Lowes, M. J. Higgins, S. E. Moulton, M. A. Murphy, M. J. Cook, G. M. Clark, G. G. Wallace and R. M. I. Kapsa, *Journal of neural engineering*, 2013, **10**, 016008.
10. L. Wan, R. Xia and W. Ding, *J Neurosci Res*, 2010, **88**, 2578-2587.
11. H. H. Liu, Y. Xiang, T. B. Yan, Z. M. Tan, S. H. Li and X. K. He, *Chinese medical journal*, 2013, **126**, 2361-2367.
12. M. Matsumoto, T. Imura, T. Fukazawa, Y. Sun, M. Takeda, T. Kajiume, Y. Kawahara and L. Yuge, *Neurosci Lett*, 2013, **533**, 71-76.
13. J. Y. Lee, J. W. Lee and C. E. Schmidt, *J R Soc Interface*, 2009, **6**, 801-810.
14. K. H. Park, H. Kim and K. Na, *J Microbiol Biotechnol*, 2009, **19**, 1490-1495.
15. L. E. Kokai, A. M. Ghaznavi and K. G. Marra, *Biomaterials*, 2010, **31**, 2313-2322.
16. G. Lamour, A. Eftekhari-Bafrooei, E. Borguet, S. Soues and A. Hamraoui, *Biomaterials*, 2010, **31**, 3762-3771.
17. B. C. Thompson, S. E. Moulton, R. T. Richardson and G. G. Wallace, *Biomaterials*, 2011, **32**, 3822-3831.
18. B. Zavan, G. Abatangelo, F. Mazzoleni, F. Bassetto, R. Cortivo and V. Vindigni, *Neurological Research*, 2008, **30**, 190-196.
19. J. Li, T. A. Rickett and R. Shi, *Langmuir : the ACS journal of surfaces and colloids*, 2009, **25**, 1813-1817.
20. D. Yucel, G. T. Kose and V. Hasirci, *Biomaterials*, 2010, **31**, 1596-1603.
21. G. C. W. de Ruiter, M. J. A. Malessy, M. J. Yaszemski, A. J. Windebank and R. J. Spinner, *Neurosurgical Focus*, 2009, **26**, E5.
22. R. Deumens, A. Bozkurt, M. F. Meek, M. A. E. Marcus, E. A. J. Joosten, J. Weis and G. A. Brook, *Progress in Neurobiology*, 2010, **92**, 245-276.
23. K. Matsumoto, K. Ohnishi, T. Kiyotani, T. Sekine, H. Ueda, T. Nakamura, K. Endo and Y. Shimizu, *Brain Research*, 2000, **868**, 315-328.
24. T. B. Bini, S. Gao, S. Wang and S. Ramakrishna, *Journal of Materials Science*, 2006, **41**, 6453-6459.
25. J. Venugopal and S. Ramakrishna, *Appl Biochem Biotechnol*, 2005, **125**, 147-158.
26. A. F. Quigley, J. M. Razal, B. C. Thompson, S. E. Moulton, M. Kita, E. L. Kennedy, G. M. Clark, G. G. Wallace and R. M. I. Kapsa, *Adv Mater*, 2009, **21**, 4393-4397.
27. X. Liu, K. J. Gilmore, S. E. Moulton and G. G. Wallace, *J Neural Eng*, 2009, **6**, 065002.
28. D. D. Ateh, H. A. Navsaria and P. Vadgama, *Journal of The Royal Society Interface*, 2006, **3**, 741-752.
29. Z. B. Huang, G. F. Yin, X. M. Liao and J. W. Gu, *Front Mater Sci*, 2014, **8**, 39-45.
30. E. Stewart, N. R. Kobayashi, M. Higgins, A. F. Quigley, S. Jamali, S. E. Moulton, R. M. Kapsa, G. G. Wallace and J. M. Crook, *Tissue Eng Part C Methods*, 2014, DOI: 10.1089/ten.TEC.2014.0338.
31. L. Forciniti, J. Ybarra, 3rd, M. H. Zaman and C. E. Schmidt, *Acta Biomater*, 2014, **10**, 2423-2433.
32. H. T. Nguyen, S. Sapp, C. Wei, J. K. Chow, A. Nguyen, J. Coursen, S. Luebben, E. Chang, R. Ross and C. E. Schmidt, *J Biomed Mater Res A*, 2014, **102**, 2554-2564.
33. H. Durgam, S. Sapp, C. Deister, Z. Khaing, E. Chang, S. Luebben and C. E. Schmidt, *J Biomater Sci Polym Ed*, 2010, **21**, 1265-1282.
34. D. Esrafilzadeh, J. M. Razal, S. E. Moulton, E. M. Stewart and G. G. Wallace, *J. Control. Release*, 2013, **169**, 313-320.
35. A. F. Quigley, J. M. Razal, M. Kita, R. Jalili, A. Gelmi, A. Penington, R. Ovalle-Robles, R. H. Baughman, G. M. Clark, G. G. Wallace and R. M. I. Kapsa, *Advanced Healthcare Materials*, 2012, **1**, 801-808.
36. *Conducting Polymers : Synthesis, Properties and Applications*, Nova Science Publishers, Inc., Hauppauge, NY, USA, 2013.
37. J. Y. Hong, H. Yoon and J. Jang, *Small*, 2010, **6**, 679-686.
38. K. U. Schirmer, D. Esrafilzadeh, B. Thompson, A. Quigley, R. I. Kapsa and G. Wallace, *J Nanopart Res*, 2015, **17**, 1-11.
39. D. Verma, P. C. Gope, A. Shandilya and A. Gupta, *T Indian I Metals*, 2014, **67**, 803-816.
40. V. Mittal, *Macromol Mater Eng*, 2014, **299**, 906-931.
41. N. Saravanan, R. Rajasekar, S. Mahalakshmi, T. P. Sathishkumar, K. S. K. Sasikumar and S. Sahoo, *J Reinf Plast Comp*, 2014, **33**, 1158-1180.
42. S. Bose, N. H. Kim, T. Kuila, K. T. Lau and J. H. Lee, *Nanotechnology*, 2011, **22**, 295202.
43. P. Si, S. J. Ding, X. W. Lou and D. H. Kim, *Rsc Adv*, 2011, **1**, 1271-1278.
44. H. P. de Oliveira, S. A. Sydlik and T. M. Swager, *J Phys Chem C*, 2013, **117**, 10270-10276.
45. I. M. D. Salas, Y. N. Sudhakar and M. Selvakumar, *Applied Surface Science*, 2014, **296**, 195-203.
46. F. H. Hsu and T. M. Wu, *Synthetic Metals*, 2014, **198**, 188-195.
47. C. Yu, P. Ma, X. Zhou, A. Wang, T. Qian, S. Wu and Q. Chen, *ACS Appl Mater Interfaces*, 2014, **6**, 17937-17943.
48. J. W. Park, S. J. Park, O. S. Kwon, C. Lee and J. Jang, *Analytical Chemistry*, 2014, **86**, 1822-1828.
49. W. D. Lin, H. M. Chang and R. J. Wu, *Sensor Actuat B-Chem*, 2013, **181**, 326-331.
50. X. Zhou, P. Ma, A. Wang, C. Yu, T. Qian, S. Wu and J. Shen, *Biosens Bioelectron*, 2015, **64**, 404-410.
51. J. Park and S. Kim, *Carbon Lett*, 2013, **14**, 117-120.
52. Y. Zhao, J. Liu, Y. Hu, H. Cheng, C. Hu, C. Jiang, L. Jiang, A. Cao and L. Qu, *Adv Mater*, 2013, **25**, 591-595.
53. M. J. Allen, V. C. Tung and R. B. Kaner, *Chem Rev*, 2010, **110**, 132-145.
54. W. Choi, I. Lahiri, R. Seelaboyina and Y. S. Kang, *Crit Rev Solid State*, 2010, **35**, 52-71.
55. S. Gambhir, R. Jalili, D. L. Officer and G. G. Wallace, *NPG Asia Mater*, 2015, **7**, e186.
56. Y. W. Zhu, S. Murali, W. W. Cai, X. S. Li, J. W. Suk, J. R. Potts and R. S. Ruoff, *Adv Mater*, 2010, **22**, 3906-3924.
57. M. O. Danilov, I. A. Slobodyanyuk, I. A. Rusetskii and G. Y. Kolbasov, *Russ J Appl Chem+*, 2013, **86**, 858-862.
58. R. Jalili, S. H. Aboutalebi, D. Esrafilzadeh, K. Konstantinov, S. E. Moulton, J. M. Razal and G. G. Wallace, *ACS Nano*, 2013, **7**, 3981-3990.
59. K. A. Mkhoyan, A. W. Contryman, J. Silcox, D. A. Stewart, G. Eda, C. Mattevi, S. Miller and M. Chhowalla, *Nano Letters*, 2009, **9**, 1058-1063.
60. S. H. Aboutalebi, R. Jalili, D. Esrafilzadeh, M. Salari, Z. Gholamvand, S. Aminorroaya Yamini, K. Konstantinov, R. L. Shepherd, J. Chen, S. E. Moulton, P. C. Innis, A. I. Minett, J. M. Razal and G. G. Wallace, *ACS Nano*, 2014, **8**, 2456–2466.
61. R. Jalili, J. M. Razal, P. C. Innis and G. G. Wallace, *Adv. Funct. Mater.*, 2011, **21**, 3363-3370.
62. C. Gomez-Navarro, J. C. Meyer, R. S. Sundaram, A. Chuvilin, S. Kurasch, M. Burghard, K. Kern and U. Kaiser, *Nano Letters*, 2010, **10**, 1144-1148.
63. S. Li, C. Zhao, K. W. Shu, C. Y. Wang, Z. P. Guo, G. G. Wallace and H. K. Liu, *Carbon*, 2014, **79**, 554-562.
64. L. Wang, M. Wang, H. Yan, Y. Yuan and J. Tian, *J Chromatogr A*, 2014, **1368**, 37-43.
65. C. H. Xu, J. Sun and L. Gao, *J Mater Chem*, 2011, **21**, 11253-11258.
66. M. Deng, X. Yang, M. Silke, W. M. Qiu, M. S. Xu, G. Borghs and H. Z. Chen, *Sensor Actuat B-Chem*, 2011, **158**, 176-184.
67. X. T. Ding, Y. Zhao, C. G. Hu, Y. Hu, Z. L. Dong, N. Chen, Z. P. Zhang and L. T. Qu, *J Mater Chem A*, 2014, **2**, 12355-12360.
68. S. P. Lim, A. Pandikumar, Y. S. Lim, N. M. Huang and H. N. Lim, *Sci Rep*, 2014, **4**, 5305.
69. Y. S. Gao, J. K. Xu, L. M. Lu, L. P. Wu, K. X. Zhang, T. Nie, X. F. Zhu and Y. Wu, *Biosens Bioelectron*, 2014, **62**, 261-267.
70. S. D. Yang, C. M. Shen, Y. Y. Liang, H. Tong, W. He, X. Z. Shi, X. G. Zhang and H. J. Gao, *Nanoscale*, 2011, **3**, 3277-3284.
71. F. H. Hsu and T. M. Wu, *Synthetic Metals*, 2012, **162**, 682-687.
72. S. H. Aboutalebi, M. M. Gudarzi, Q. B. Zheng and J.-K. Kim, *Adv. Funct. Mater.*, 2011, **21**, 2978-2988.
73. R. Jalili, S. H. Aboutalebi, D. Esrafilzadeh, R. L. Shepherd, J. Chen, S. Aminorroaya-Yamini, K. Konstantinov, A. I. Minett, J. M. Razal and G. G. Wallace, *Advanced Functional Materials*, 2013, **23**, 5345-5354.
74. R. Jalili, S. H. Aboutalebi, D. Esrafilzadeh, K. Konstantinov, J. M. Razal, S. E. Moulton and G. G. Wallace, *Mater. Horiz.*, 2014, **1**, 87-91.
75. A. T. C. Collection, http://www.atcc.org/products/all/CCL-1.aspx#culturemethod).

Journal of Materials Chemistry B RSCPublishing

ARTICLE

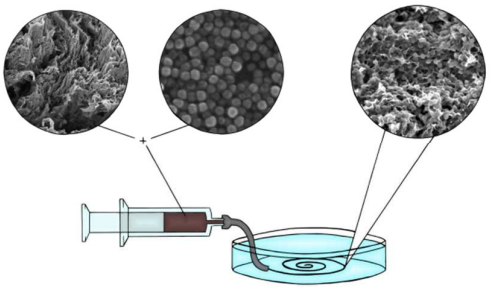

Wet-spun composite fibres from graphene and polypyrrole nanoparticles show appropriate mechanical properties, high electrical conductivity and good cytocompatibility.